An integrative model of chimera jaw links mechanical stress to localized cartilage mineralization

Francois Clarac, A Sanchez-Gimeno, A Quilhac, A Herrel, Q Grimal, A Pradel

An integrative model of chimera jaw links mechanical stress to localized cartilage mineralization

F. Clarac[1], A. Sanchez-Gimeno[1], A. Quilhac[1], A. Herrel[2,3,4,5], Q. Grimal[6], A. Pradel[1]

[1]CR2P, Centre de Recherche en Paléontologie–Paris, Muséum National d'Histoire Naturelle, Sorbonne Université, Centre National de la Recherche Scientifique, CP 38, Paris Cedex 05, F75231

[2]Mécanismes Adaptatifs et Evolution, UMR 7179, Muséum National d'Histoire Naturelle CNRS, Paris, France

[3] Department of Biology, Evolutionary Morphology of Vertebrates, Ghent University, Ghent, Belgium

[4] Department of Biology, University of Antwerp, Wilrijk, Belgium

[5] Naturhistorisches Museum Bern, Bern, Switzerland

[6]Sorbonne Université, INSERM UMR-S 1146, CNRS UMR 7371, Laboratoire d'Imagerie Biomédicale, 75006 Paris, France

Corresponding author: François CLARAC, 43 rue Buffon 75005 Paris, France, francois.clarac@mnhn.fr

Abstract

Chondrichthyans possess a tessellated cartilage which is characterized by a layer of mineralized minute plates (*i.e.* the tesserae) that sheathe soft cartilage. This tissue type composes most of the endoskeleton (including the fins, the branchial arches and the skull). Using the example of the adaptation of Holocephalans to durophagy, here we aim to test the capacity of the tessellated cartilage to strengthen in response to mechanical stress. Relying on an integrative approach (*i.e.* cranial muscle dissections, finite element models, histological cross sections and embryologic data), we strongly argue that chondrichthyans are capable of calcifying their endoskeleton in response to mechanical stress by mimicking bone microstructures (*i.e.* cortical thickness and formation of trabeculae). In absence of bone cells, this mechanism relies on the calcification of Liesegang waves around the chondrocytes that might possess mechanosensing properties. This cartilage ability may have been inherited from the early jawless vertebrates before it played a critical role in the evolution of chondrichthyans who subsequently lost the bony skeleton before thriving through 400 million years and surviving four major extinction crises. Indeed, this ability to mineralize cartilage would have allowed to grow a high diversity of mechanically demanding adaptations within "bone-less" vertebrates.

Résumé

Les chondrichtyens possèdent un cartilage tessellé qui se caractérise par une strate de petites plaques minéralisées (*i.e.* les tesselles) recouvrant le cartilage hyalin. Ce type de tissu compose la majeure partie de l'endosquelette (y compris les nageoires, les arcs branchiaux et le crâne). En prenant l'exemple de l'adaptation des Holocéphales à la durophagie, nous visons à tester la capacité du cartilage tessellé à se renforcer en réponse au stress mécanique. En nous appuyant sur une approche intégrative (incluant des dissections des muscles crâniens, des analyses en éléments finis, des coupes histologiques et des données embryologiques), nous soutenons que les chondrichtyens sont capables de calcifier leur endosquelette en réponse au stress mécanique en imitant les microstructures osseuses (*i.e.* l'épaississement cortical et la formation de trabécules). En l'absence de cellules osseuses, ce mécanisme repose sur la calcification d'anneaux de Liesegang autour des chondrocytes, qui pourraient ainsi posséder des propriétés de mécanoréceptrices. Cette capacité du cartilage pourrait alors avoir été héritée des premiers vertébrés sans mâchoires avant de jouer un rôle crucial dans l'évolution des chondrichtyens, qui ont perdu le squelette osseux avant de prospérer au travers de 400 millions d'années et à survivre à quatre crises d'extinctions majeures. En effet, une telle propriété cellulaire aurait permis le développement d'une grande diversité d'adaptations biomécaniques chez des vertébrés « sans os ».

Keywords

Biomechanics, Chondrocyte, Evolution, Durophagy, Trabeculae, Finite Element Analysis, Microanatomy

Mots-clefs :

Biomécanique, Chondrocyte, Evolution, Durophagie, Trabécules, Analyse en éléments finis, Microanatomie

Introduction

The chondrichthyans are the extant representatives of a 400-million-year-old vertebrate group that probably originated from the acanthodians during the Silurian (Maisey et al. 2017, Coates et al.2018). They further diversified during the Devonian within two separate sub-groups: the elasmobranchs and the holocephalans (Grogan et al. 2012, Boisvert et al. 2019), which both share a cartilaginous skeleton that calcifies following one of two distinct patterns (Debiais-Thibaud 2019): 1) the areolar cartilage that grows in centrifugal concentric circles within the center of the vertebrae (Atake et al. 2019, 2024); 2) the tessellated cartilage which is basically characterized by a layer of mineralized minute plates (*i.e.* the tesserae) that sheathe the cartilage and compose most of the endoskeleton, including the fins, the branchial arches and the skull (Dean & Summer 2006, Seidel et al. 2020). However, previous studies have shown that the tesserae differ in their size, structure, and organization (Maisey et al. 2021, Seidel et al. 2021), as they result from either a prismatic mineralization that is usually associated to the perichondrium (Dean & Summer 2006) or from a globular calcification that surrounds the chondrocytes within the extracellular matrix (Kemp & Westrin 1979). At a microanatomical level, the association of both prismatic and globular calcification may form either a cortex that can be made of multiple-monolayered or polylayered tesserae (Dingerkus et al. 1991, Dean et al. 2009, Maisey et al. 2021, Pazzaglia et al. 2022A, Pazzaglia 2022B) or a set of trabeculae (also named « struts ») that cross the uncalcified cartilage to further interconnect the external tesserae layers (Summers 2000, Seidel et al. 2017, Atake et al. 2019). These two latter microstructures suggest an analogy with bone microanatomy (Swartz et al. 1998). Therefore, some authors hypothesized that their function is to strengthen the cartilage in response to external mechanical constraints (Dean & Summer 2006). Indeed, even if the cortical thickening commonly reduces bending stress in most elasmobranch species (Dingerkus et al. 1991, Clark et al. 2022), trabeculae may also play a more specific role in the reinforcement of the jaw in durophagous taxa (*e.g.* myliobatid stingrays; Summers 2000, Seidel et al. 2017). Like the durophagous batoid elasmobranchs, the holocephalans (*i.e.* the sister group of elasmobranchs) are specialized in hard-prey crushing, as evidenced by the combined presence of both dental plates (Johanson et al. 2021) and strong jaw adductor muscles (Huber et al. 2008).

Here we focus on the lower jaw (*i.e.* Meckel's cartilage) of *Chimaera monstrosa* to test the role of both cortical thickening and the presence of trabeculae in absorbing the mechanical stress due to the contraction of the jaw adductor muscles and the compression from biting transmitted by the dental plates to Meckel's cartilage during hard-prey crushing (Huber et al. 2008). To do so, we use a combination of finite element models of the calcified Meckel's cartilage (Fig. 1) and histological cross sections in order to explore the possible link between mechanical stress and the development of microanatomical structures (*i.e.* cortical thickness, trabecular structures) in the tessellated cartilage. Specifically, we ask: do the chondrocytes possess a mechanosensing property (Williantarra et al. 2022) allowing to strengthen the chondrichthyan cartilage by calcification (Takagi et al. 1984, Hara et al. 2018; *i.e.* either via cortical thickening or trabecular reticulation) in response to external loading? Beyond the adaptation to hard-prey crushing in holocephalans, such a cartilage property might further be at the origin of a large set of adaptive morphological traits that were useful to respond to external stress throughout 400 million years of evolution (Burrow & Blaauwen 2021).

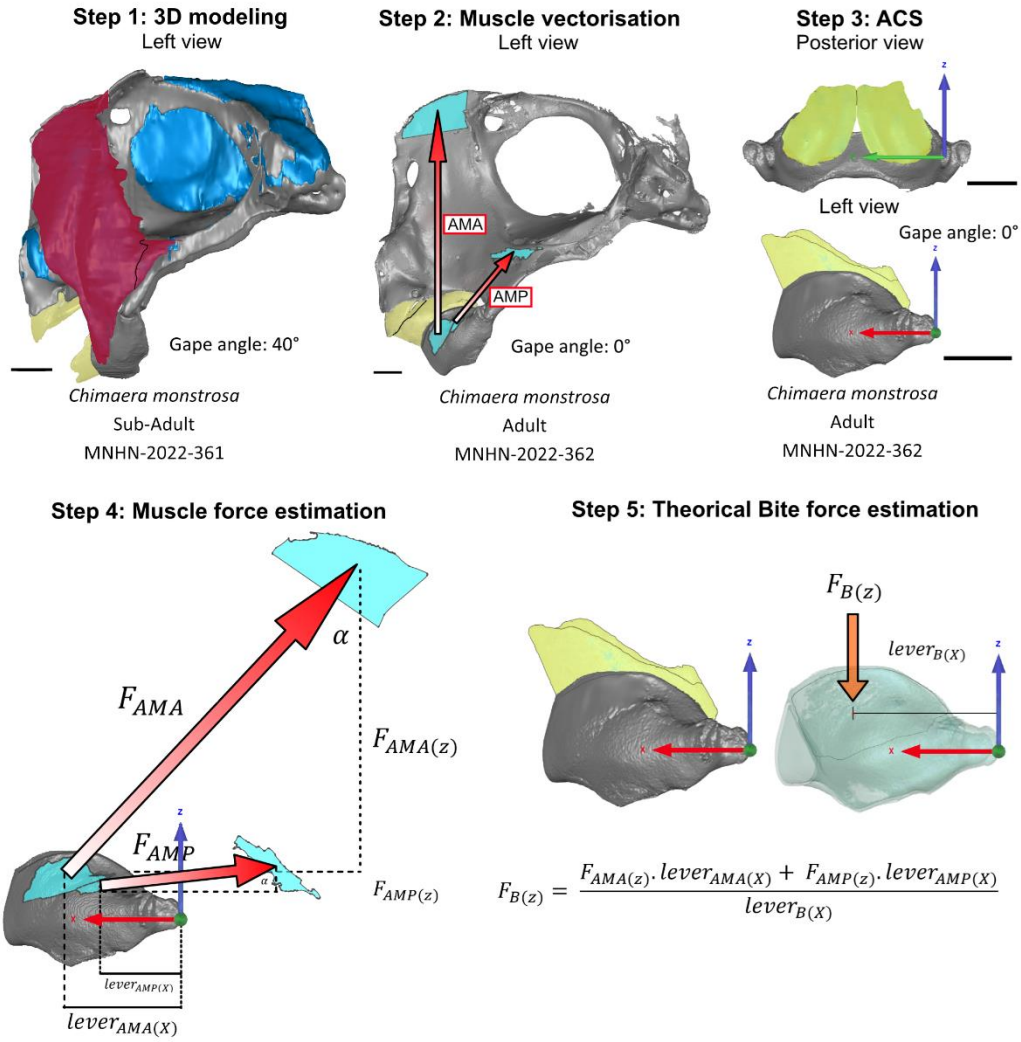

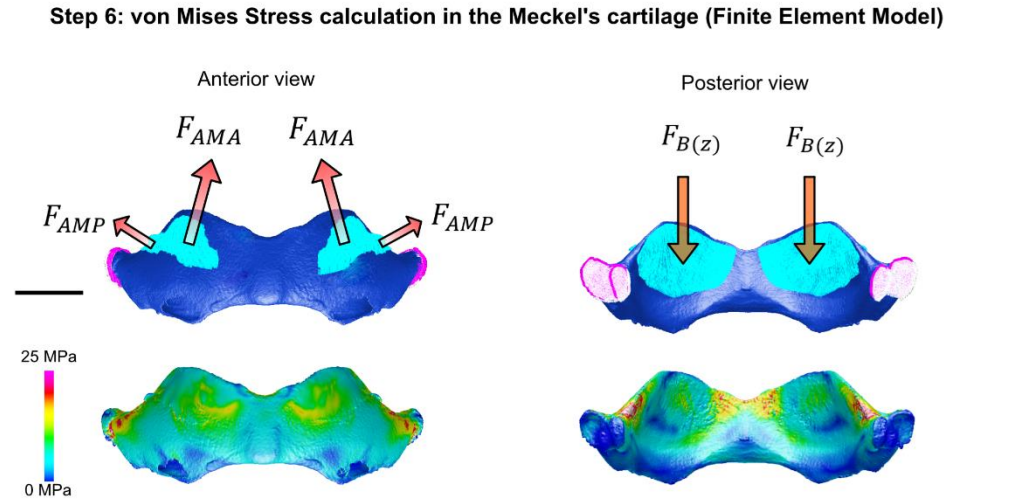

Figure 1: Determination of the mechanical stress in the lower jaw (Meckel's cartilage) due to biting in *Chimaera monstrosa* (Holocephali). Scale bars: 1 cm. Abbreviations: AMA: Adductor Mandibulae Anterior, AMP: Adductor Mandibulae Posterior, ACS: Anatomical Coordinate System. See "material and methods" for details.

Material and methods

Sample

We sampled three specimens that belong to *Chimaera monstrosa* (Holocephali): one juvenile (skull length: 68mm) which was collected in 2005 by Alan Pradel during an IFREMER mission (under the funding of John G. Maisey) in the Gulf of Gascony (Atlantic ocean); one sub-adult (MNHN-2022-361; skull length: 95mm) and one fully mature specimen (MNHN-2022-362; skull length: 115mm), which were also captured in the Atlantic Ocean and gathered by the marine station of Concarneau (Muséum National d'Histoire Naturelle, Quai de la Croix, 29900 Concarneau, France). All specimens were preserved in ethanol (70°). We scanned both the sub-adult (MNHN-2022-361) and the fully mature specimen (MNHN-2022-362) at the µCT scan platform (AST-RX) of the Muséum National d'Histoire Naturelle at a voxel size of 71 µm. Before scanning, the sub-adult specimen (MNHN-2022-361) was placed in a contrast agent (phosphomolybdic acid, 5%) to reconstruct the cranial muscles in 3D (see below).

3D-modelling

We modeled both the sub-adult (MNHN-2022-361) and the adult specimen (MNHN-2022-362) using segmentation software (Mimics 21.0.0.0.46, Materialise license, Technologielaan 153001 Leuven Belgique). For the adult specimen we segmented the calcified cartilage which is distinguishable by its high contrast on the tomographic slides. As we previously stained the sub-adult specimen (MNHN-2022-361) with phosphomolybdic acid, we also segmented the muscles that are involved in the jaw adduction (*i.e.* the anterior adductors and the posterior adductors).

In order to export watertight STL files to build a FE model of the lower jaw (Meckel's cartilage), we repeated the segmentation using VG Studiomax (version 3.1; Speyerer Straße 4-6 69115 Heidelberg Germany). We thus created: 1) one realistic model which includes all the calcified cartilage (*i.e.* with the trabeculae that interconnect the tesserae and external collar) 2) one virtual model that only consists of the tessellated external collar. We cleaned the exported mesh by correcting the remaining problems using Geomagic Wrap 2021 (version 2.1; Artec 3D, 4 Rue Lou Hemmer, L-1748 Senningerberg (Headquarters) 11 Breedewues, Luxembourg) before we exported a final STL file for further importation into a Finite Element software (Strand7 R 3.1.3, Suite 1, Level 565 York Street Sydney NSW 2000 Australia). We finally created a volume tetrahedral mesh on Strand7 for both models, each of which is composed of more than 37 million of bricks (tetrahedrons).

Muscle forces

We dissected the adult specimen (MNHN-2022-362), which we further used for finite element models. In order to facilitate the dissection, we previously fixed the specimen in a 10% formaldehyde solution for 48 hours, rinsed it overnight and transferred it to a 70% aqueous ethanol solution. We dissected and weighed the muscles after removing the excess of alcohol. Muscles were transferred to petri dishes which were filled with nitric acid (30% in water) in order to separate the muscle fibres. After a period of 24 hours, we removed the nitric acid from the petri dish and added a 50% aqueous glycerol solution to arrest fibre digestion. We finally separated the fibres with the use of tweezers and needles so we measured 10 fibres per muscle in order to calculate their mean length. Within the same step, we measured the pennation angle (θ). We subsequently calculated the physiological cross section area (P_{CSA}; Supplementary Table 1) of each muscle and deducted the theoretical maximum tetanic force (P_o).

$$P_{CSA} = \frac{musclemass}{muscledensity}.cos\theta.\frac{1}{fiberlength},$$

$$P_o = P_{CSA}.T_{SPR}.$$

With a gnathostome muscle density value of 1.05 g.cm^{-3} (Powell et al. 1984, Wainwright 1988, Huber et al. 2008) and the specific tension of elasmobranch red muscle (T_{SPR} = 142 kN.m^{-2} ; Lou et al. 2002).

Theoretical bite force

Using Geomagic Wrap, we imported a STL file of both the lower jaw (Meckel's cartilage), the upper jaw (fused neurocranium and palatoquadrate) and the dental plates of the adult specimen (MNHN-2022-362) at a gape angle of 0°; we then created an anatomical coordinate system (ACS). We defined the origin of the system at the left joint between the lower jaw and the upper jaw, the X axis is defined toward the anterior part of the lower jaw, the Y axis is defined by the lateral axis between the left to the right joint, the Z axis is orthogonal to Y and X and points dorsally. We then imported and scaled both the anterior and the posterior adductor muscles from the sub-adult specimen (MNHN-2022-361) so we could define both the muscle insertion and origin areas on the adult specimen skull via a Boolean operation (*i.e.* intersection between two objects). We then defined the centroid of these intersection areas with the dedicated tool so we could model the muscles as vectors and further compute both their length and orientation relative to each axis (X, Y, Z). We could thus deduce the force component of each muscle along each axis (X, Y, Z) when the gape angle is 0° (Fig. 1 Step 1-4, Supplementary Table 2):

$$P_{o(X,Y,Z)} = P_o cos\alpha_{(X,Y,Z)}$$

With α the angle between the muscle vector and each axis at the muscle insertion on the lower jaw. We repeated the upper Boolean operation between the Meckel's cartilage and the dental plate in order to determine their intersection. We could then calculate the theoretical bite force at the centroid of the intersection area when the gape angle is 0°, using the following formula (Fig. 1 Step 4-5):

$$F_{B(z)} = \frac{F_{AMA(z)}.lever_{AMA(X)} + F_{AMP(z)}.lever_{AMP(X)}}{lever_{B(X)}}$$

With "lever" the distance between each centroid and the origin of the ACS along the X axis.

Finite Element Model

After we created the 3D-volume mesh on Strand 7, we imported the perimeter of the 6 intersection areas (IGES files) in order to circle and identify the nodes on which we applied the forces (Fig. 1 Step 6). We previously determined the component of each muscle force along the 3 ACS axes (X, Y, Z) using a trigonometric formula:

$$F_{M(X,Y,Z)} = F_M cos\alpha_{(X,Y,Z)}$$

Where α is the angle between the muscle force vector and the ACS axes (X, Y, Z). The calculated force components are summarised in Supplementary Table 2.

To apply the theoretical bite force on the intersection area between the Meckel's cartilage and each dental plate, we considered that the resulting force acts only vertically along the Z axis since the gape angle is 0° (Fig. 1 Step 3-5).

$$F_{B(X)} = 0; F_{B(Y)} = 0; F_{B(Z)} = F_B = 22.85 \text{ N}$$

We imposed zero nodal displacement to the elements of the joint area that contact the palatoquadrate (upper jaw). We disregard the stress absorption effect of the hyaline cartilage which homogeneously surrounds the calcified cartilage both on the outer and the inner part of the tessellated collar (see Fig 3. C1). We also disregard the part of the bite force component that should be partly absorbed by the dental plate that has a very complex structure (Smith et al. 2020).

Since our purpose here is to compare the mechanical effect of the struts, we repeated the same analysis over two versions of the same model by including one in which the trabeculae have been artificially removed (as explained above). We calculated both the three-dimensional displacement of the tetrahedral bricks (*i.e.* the finite elements) and the von Mises criterion (a scalar measure encompassing the whole 3D stress state, which is commonly used to define a strength criterion in terms of the maximum distortion of a ductile material; Fig. 1 Step 6) after setting a Young modulus of (E = 4.05 GPa) and a Poisson ratio of 0.30 (Wroe et al. 2008). In order to assess the sensitivity of our results to the choice of the mechanical properties, we repeated the calculation with a much higher Young modulus (E = 40 GPa). We noticed no difference in the results (*i.e.* von Mises stress). We ran a Linear Static Analysis (LSA, which involves a small deformation with no change of loading with time), a sparse storage scheme, an AMD sorting method and an Iterative Preconditioned Conjugate Gradient (PCG) solution type. After solving the finite element model, we exported the displacements and the mean stress calculated for each finite element (in a .txt format). We opened this file with R 4.0.0 (CRAN; R Core team) and ran a Wilcoxon signed-rank test to compare both the median brick von Mises stress and the median brick displacement between the two models. We estimated that this non-parametric statistical test which aims to compare the median value between two paired groups was suitable since the data should not follow a normal distribution in our model. Indeed, we compare the median stress between two populations that are made of interconnected finite elements (Clarac et al. 2024). Both the brick displacement and stress values are summarized in Table 1.

A

Brick	Min	1st Qu.	Median	Mean	3rd Qu.	Max
Stress (MPa)	0	0.3693	**0.9002**	1.4342	1.8566	197.5030
Displ. X (mm)	0	0.003421	**0.023854**	0.038097	0.065983	0.154583
Displ. Y (mm)	0	0.004677	**0.017300**	0.047484	0.081410	0.224477
Displ. Z (mm)	0	0.006125	**0.020331**	0.021307	0.032731	0.067055

B

Brick	Min	1st Qu.	Median	Mean	3rd Qu.	Max
Stress (MPa)	0	1.151	**2.685**	4.672	5.645	516.138
Displ. X (mm)	0	0.04638	**0.13430**	0.15866	0.24928	0.52995
Displ. Y (mm)	0	0.009794	**0.020331**	0.021307	0.032731	0.067055
Displ. Z (mm)	0	0.3512	**0.7825**	0.7462	1.1477	1.5842

C

Brick	W	P-value
Stress (MPa)	5.7783e+14	< 2.2e-16***
Displ. X (mm)	7.617e+13	< 2.2e-16***
Displ. Y (mm)	5.9894e+13	< 2.2e-16***
Displ. Z (mm)	6.8802e+12	< 2.2e-16***

Table 1: Statistical summary of the von Mises stress and brick displacements in the lower jaw (Meckel's cartilage) of *Chimaera monstrosa* (MNHN-2022-362). A. The realistic model which includes all the calcified cartilage (*i.e.* the trabeculae that interconnect within the tesserae external collar). B. The modified model that only consists of the tessellated external collar. X is the longitudinal axis, Y is the lateral axis, Z is the vertical axis (shown in Figure 1 and detailed in Material and Methods). C. Wilcoxon rank test comparison between the model A and the model B.

Histological sections for light microscopy

We performed semi-thin sections on the lower jaw of the juvenile specimen, which we fixed in 2.5% glutaraldehyde, 2% paraformaldehyde in 0.1 mol/l cacodylate buffer after removing most of the flesh. The samples were demineralized with 5% EDTA added in the fixative. The demineralized samples were dehydrated and subsequently embedded in Epon. Semi-thin sections (100 microns thick) stained with toluidine blue were examined by light microscopy. We then performed paraffin sections on lower jaw samples of the fully mature specimen (MNHN-2022-362), which we fixed in a Bouin's mixture, dehydrated in butanol, and embedded in paraffin. The sections were stained with Masson's trichrome (as in Marconi et al. 2020). For both semi-thin and paraffin sections, the lower jaw cartilage was longitudinally and transversely sectioned.

Results

The contraction of the adductor muscles combined with the reaction force on the jaw at the bite point results in a high stress on the posterior dorsal region of the Meckel's cartilage toward the lower jaw joint (Fig. 2A). To assess the consequences of mechanical stress from a histological point of view, Masson's trichrome staining is particularly suitable. Mineralized cartilage is stained pink, contrasting with non-mineralized hyaline cartilage stained in blue (Fig. 3B). In addition, there is a gradation of pink depending on the degree of mineralization. In this way, we were able to highlight cartilage mineralization in a precise spatio-temporal manner. Areas of constraints are obviously reinforced by a cortical thickening of the calcified tessellated collar, which likely helps absorb the high stress. Notable is the development of globular cartilage which grows from the tesserae monolayer to the perichondrium (Fig. 2A4 Cross section 1; Fig. 3B1). The stress is also high in the anterior dorsal region of the lower jaw, likely as a result of the shearing constraints that are due to the combined tensile forces generated by the adductor muscles and the compression of the dental plate where the stress is absorbed by the trabeculae (or "struts") that interconnect the external tessellated collar (Fig. 2A4 Cross section 2). These trabeculae are set up through the development of globular cartilage that grows from the hyaline cartilage matrix that is enclosed in the tessellated collar (Fig. 3B3). Mineralization progresses from the tesserae towards the center of the collar. Both mineralization fronts join to form parallel highly mineralized trabeculae interspersed with hyaline cartilage. These trabeculae do not only absorb the local stress but also maintain the overall lower jaw structure. Indeed, the finite element model on which we artificially removed the trabeculae (Fig. 2B) shows an extension of the high stress area over the ventral region of the lower jaw (where the external tessellated collar is only made up of a tesserae monolayer; Fig. 2B; Fig. 3B2). The finite element analysis shows that the removal of the trabeculae provokes an increase of the median von Mises stress from 0.90 MPa to 2.69 MPa and a higher brick displacement mainly along the vertical axis (Z) and secondarily along the longitudinal axis (X) (Table 1, Supplementary Figure 1).

Cortical thickening and trabeculae development involve the same process of globular cartilage growth, which is observable from the juvenile stage (Fig. 3C). This growth is initiated by the chondrocytes that are located in the hyaline cartilage either distally between the tessellated collar and the perichondrium or proximally within the tessellated collar (Fig. 3C2). The combined individual action of each chondrocyte results in the connection of various irregular calcified blocks (Fig. 3C2) that will eventually shape up as bone-like microstructures (Fig. 3B1, B3). The chondrocytes will be progressively surrounded by several concentric layers of calcified cartilage before they may eventually die (Fig. 3C3). As calcification progresses, the tesserae may lose their cuboidal shape and merge with newly formed calcified blocks (Fig. 3B3). At this later stage, it is difficult to delimit the tesserae which seem to have fused with neighboring elements (Fig. 4).

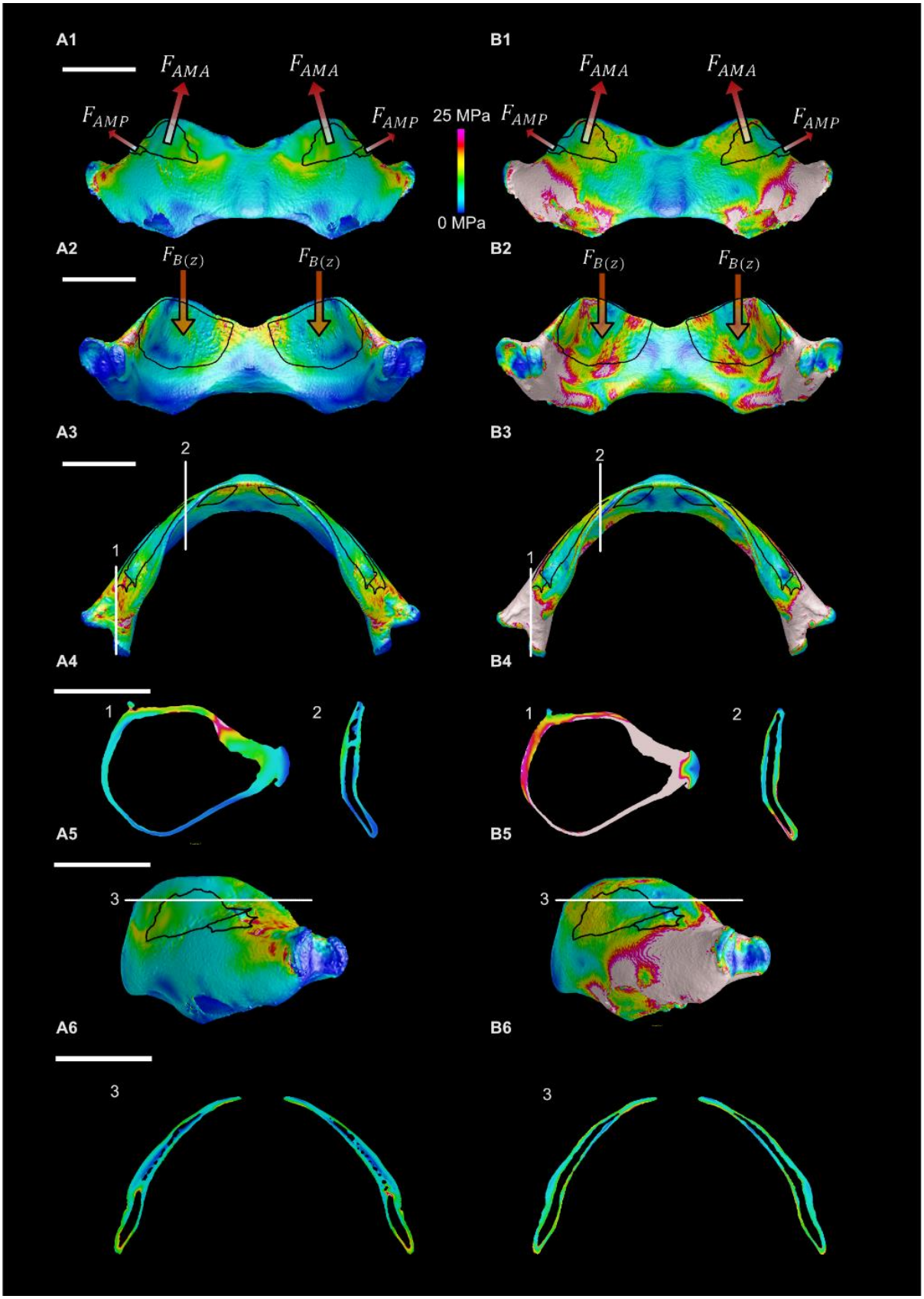

Figure 2: Distribution of the von Mises stress in the lower jaw (Meckel's cartilage) due to biting in the adult specimen of *Chimaera monstrosa* (MNHN-2022-362). A) The realistic model that includes all the calcified cartilage (*i.e.* the trabeculae that connect the tesserae within the external collar). B) The modified model that only consists of the tessellated external collar. A1-B1: Anterior view, A2-B2: Posterior view, A3-B3: Dorsal view,

A4-B4: Transversal cross-sectional views, A5-B5: Left lateral view, A6-B6: Longitudinal cross section. Scale bars: 1cm. The black lines delimit the areas where the forces were applied (*i.e.* on the labial regions: the jaw adductor muscle insertions; on the lingual regions: the dental plate insertions).

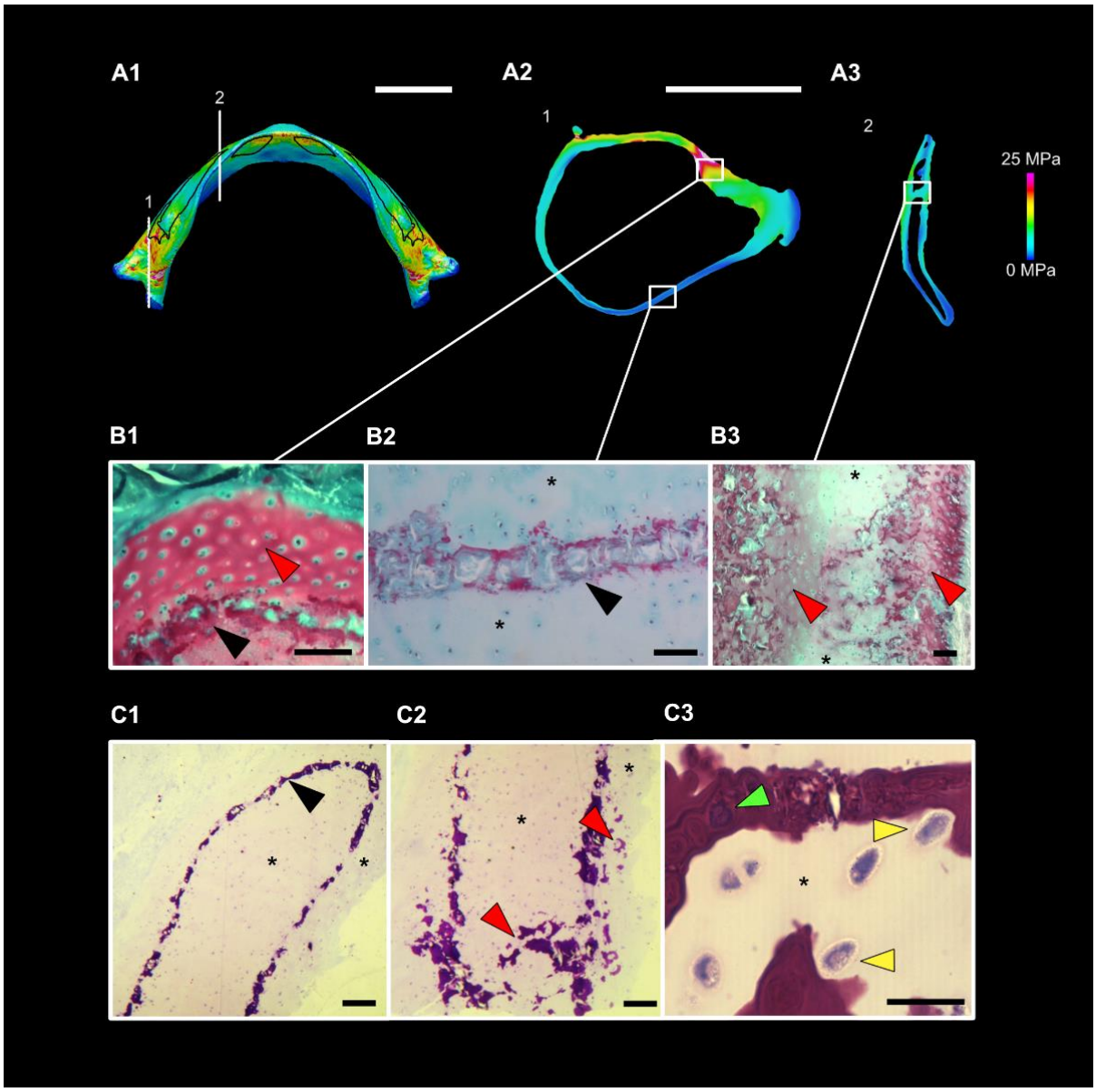

Figure 3: The tessellated cartilage reinforcement process. A. Transverse cross-sectional views of the von Mises stress in the lower jaw (Meckel's cartilage) of the adult specimen of *Chimaera monstrosa* (MNHN-2022-362). A1: Full dorsal view, A2-A3: Transversal cross-sectional views. Scale bar: 1cm. B. Histological cross sections of the adult specimen of *Chimaera monstrosa* (MNHN-2022-362). B1. Cortical thickening, B2: Single tesserae layer, B3: Trabeculae. Scale bars: 100µm. The Masson's trichrome colorant stains in pink: the mineralized cartilage, in blue: the hyaline cartilage, in green: the perichondrium. C. Histological cross sections of the juvenile specimen of *Chimaera monstrosa*. C1: Monolayered tesserae collar. Scale bar: 100µm. C2. Cortical thickening and trabeculae setting. Scale bar: 100µm. C3: Chondrocyte mineralization. Scale bar: 10µm. The toluidine stains in purple: the calcified cartilage, in deep blue: the chondrocytes. Red arrows: Globular cartilage calcification, Black arrows: Monolayer of tesserae, Yellow arrow: Chondrocyte mineralization, Green arrow: Dying chondrocyte after growing several rings of calcified cartilage (called Liesegang waves), Asterisk: Hyaline cartilage.

Discussion

Our results suggest that the post-hatching mineralization of the holocephalan lower jaw is built in response to the mechanical stress that is induced by hard-prey crushing. Observations on *Callorhinchus callorhynchus* (Holocephali) show that there are no trabeculae in the lower jaw of neither pre-hatching nor hatchling specimens (Supplementary Figure 2) whereas they are present in adults. Therefore, unless the Liesegang waves mineralize along a pre-established late developmental pattern, the holocephalan jaw chondrocytes shall possess a mechanical sensing property (Williantarra et al. 2022) that allows to calcify the cartilage (Kemp and Westrin 1979, Takagi et al. 1984, Hara et al. 2018) in response to the recurrent external loading associated with hard-prey crushing. Such a cellular mechanism would be key in the evolution of Chondrichthyes since they are assumed to have lost (Rineau et al. 2015) their bony skeleton during the Silurian (Pradel et al. 2014, Coates et al.2018, Frey et al. 2020). Indeed, this would provide a mechanism allowing to mineralize their hyaline cartilage in response to external loading without the action of bone cells. Moreover, in contrast to bone growth and remodeling that relies on a blood vessel network (Zoetis et al. 2003), the cartilage calcification does not need any vascular supply and might thus require less metabolic energy (De Paula & Rosen 2013). Even though our results show that the tesserae layers are difficult to identify in some secondarily calcified areas (*i.e.* at the base of the trabeculae; Fig. 3B3), we cannot so far demonstrate any cell resorption activity that targets the calcified cartilage in analogous way to bone resorption which allows secondary bone remodeling in bony skeleton vertebrates (Teitelbaum 2000).

The mineralizing chondrocyte abilities likely permits a large spectrum of morphologies that could be at the origin of putative functional adaptations that rely on the jaw cartilage reinforcement via local calcification (Dingerkus et al. 1991, Clark et al. 2022). For instance, within the early holocephalans, some species are known to be durophagous and to possess similar "struts" in the upper jaw (*i.e. Helodus*; Johanson et al. 2021, Coates et al. 2021), whereas others, such as *Iniopera* sp. are thought to be suction feeders (Late Carboniferous, 305-299Ma; Dearden et al. 2023), which is the type of feeding that is the least mechanically constraining since the jaws are not involved in food prehension. Within this extinct form, we observed the absence of both cortical thickening and trabeculae within the lower jaw that is instead only composed of continuous monolayered tesserae (Supplementary Figure 3). These observations suggest that the acquisition of such microanatomical features went hand in hand with the adaptation to durophagy in holocephalans. The independent convergence of these traits in both holocephalan and the elasmobranch durophagous taxa (*e.g.* the myliobatid stingrays; Summers et al. 1998; the hybodontid sharks; Lane & Maisey 2012) is made possible by the plasticity of the chondrichthyan tessellated cartilage. The chondrocyte biomineralization abilities likely originated in acanthodians (Burrow & Blaauwen 2021) or even perhaps in early jawless vertebrates since globular calcified cartilage has been documented in at least some of them (*e.g. Atraspis*; Lemierre & Germain 2019). Such a cell property would have subsequently allowed to strengthen parts of the skeleton subjected to major mechanical stress to grow mechanically demanding adaptations within "bone-less" vertebrates over 400 million years ago.

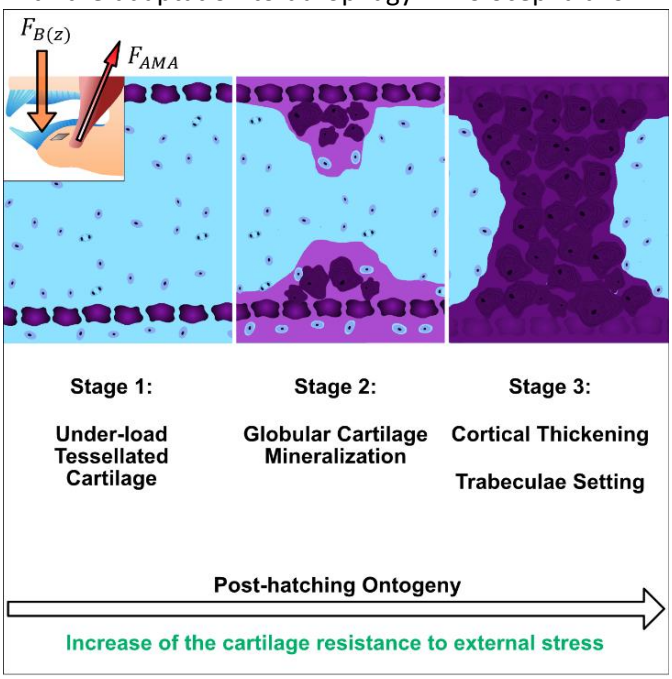

Figure 4: Summary of the cartilage mechanosensing mineralization hypothesis in the holocephalan jaw. In blue: the hyaline cartilage, in light purple: the cartilage under calcification, in dark purple: the calcified cartilage.

Acknowledgments

This research project was supported by the ANR-22-CE02-0015-01_MACHER which was obtained by Dr. Alan Pradel (Curator at the Muséum National d'Histoire Naturelle) in collaboration with Prof. Quentin Grimal (Sorbonne Université) and Prof. Anthony Herrel (Muséum National d'Histoire Naturelle). We thank both Hayat Lamrous (Lab technician at the Centre de Recherche de Paléontologie-Paris) for preparing the histological cross sections and our 3D-platform engineers (Florent Goussard and Nathalie Poulet-Crovisier) for helping with the installation of the software. We send our respectful regards to both Prof. Mickael Coates for sharing CT-scan data of the skull of *Helodus simplex* (NHMUK PV P8212) and Prof. Adam Summers for sharing raw images of the specimen SIO 64-483, which was scanned by Matt Kolmann at the Scripps Museum (California, USA). We also wish to acknowledge all the participants who were involved in the collecting of the specimens: Samuel Iglesias (station marine de Concarneau, Muséum National d'Histoire Naturelle), Robert Bellail (station marine de la Rochelle-L'Houmeau, Ifremer), Edgardo Ernesto Di Giacomo (Station Marine de San Antonio Oeste, Rio Negro, Instituto de Biologia Marina y Pesquera Almirante Storni de la Universidad de Comahue).

References

ATAKE O., COOPER D.M.L., EAMES B.F., 2019. Bone-like feature in skate suggest a novel elasmobranch synapomorphy and deep homology of trabecular mineralisation patterns. *Acta Biomaterialia* 84: 424-436. https://doi.org/10.1016/j.actbio.2018.11.047

ATAKE O.J., BERIO F., DEBIAIS-THIBAUD M., EAMES B.F., 2024. Extant cartilaginous fishes share trabecular and areolar mineralisation patterns, but not tesserae, and evidence for a paedomorphic chimaera skeleton. *arXiv* https://doi.org/10.1101/2024.01.07.574539

BERIO F., BROYON M., ENAULT S., PIROT N., LÓPEZ-ROMERO F.A., DEBIAIS-THIBAUD M., 2021. Diversity and evolution of mineralised skeletal tissues in chondrichthyans. *Frontiers in Ecology and Evolution* 9: 660767. https://doi.org/10.3389/fevo.2021.660767

BOISVERT C.A., JOHNSTON P., TRINAJSTIC K., JOHANSON Z., 2019. Chondrichthyan evolution, diversity, and senses, *in* ZIERMANN J.M., DIAZ R.E. Jr, DIOGO R. (eds), *Heads, Jaws, and Muscles*, Berlin, Germany: Springer International Publishing, Fascinating Life Sciences, pp. 65–91.

BURROW C.J., BLAAUWEN J.L., 2021. Endoskeleton tissues of acanthodians (Stem Chondrichthyes), *in* PRADEL A., DENTON J.S.S., JANVIER P. (eds), *Ancient Fishes and Their Living Relatives: A Tribute to John G Maisey*, Munich, Germany: Verlag Dr. Freidrich Pfeil, pp. 81-91.

CLARAC F., CORNILLE A., BIJL S., SANCHEZ S., 2024. Tetrapod terrestrialisation: a weight-bearing potential already present in the humerus of the stem-tetrapod fish *Eusthenopteron foordi*. *arXiv* 579723. https://doi.org/10.1101/2024.02.09.579723

CLARK B., CLARK B., CHAUMEL J., JOHANSON Z., UNDERWOOD C., SMITH M.M., DEAN M.N., 2022. Bricks, trusses and superstructures: Strategies for skeletal reinforcement in batoid fishes (rays and skates). *Frontiers in Cell and Developmental Biology* 10: 932341. https://doi.org/10.3389/fcell.2022.932341

COATES M.I., FINARELLI J.A., SANSOM I.J., ANDREEV P.S., CRISWELL K.E., TIETJEN K., RIVERS M.L., LA RIVIERE P.J., 2018. An early chondrichthyan and the evolutionary assembly of a shark body plan. *Proceedings of the Royal Society B* 285: 20172418. https://doi.org/10.1098/rspb.2017.2418

COATES M.I., TIETJEN K., JOHANSON Z., FRIEDMAN M., SANG S., 2021. The cranium of *Helodus simplex* (Agassiz, 1838) revised, *in* PRADEL A., DENTON J.S.S., JANVIER P. (eds), *Ancient Fishes and Their Living Relatives: A Tribute to John G Maisey*, Munich, Germany: Verlag Dr. Freidrich Pfeil, pp. 193-204.

DE PAULA F.J.A., ROSEN C.J., 2013. Bone remodeling and energy metabolism: new perspectives. *Bone Research* 1: 72–84. https://doi.org/10.4248/BR201301005

DEAN M.N., SUMMERS A.P., 2006. Mineralised cartilage in the skeleton of chondrichthyan fishes. *Zoology* 109: 164–168. https://doi.org/10.1016/j.zool.2006.03.002

DEAN M.N., MULL C.G., GORB S.N., SUMMERS A.P., 2009. Ontogeny of the tessellated skeleton: insight from the skeletal growth of the round stingray *Urobatis halleri*. *Journal of Anatomy* 215: 227–239. https://doi.org/10.1111/j.1469-7580.2009.01116

DEARDEN R.P., HERREL A., PRADEL A., 2023. Evidence for high-performance suction feeding in the Pennsylvanian stem-group holocephalan *Iniopera*. *Proceedings of the National Academy of Sciences* U.S.A. 120: e2207854119. https://doi.org/10.1073/pnas.2207854119

DEBIAIS-THIBAUD M., 2019. The evolution of endoskeletal mineralisation in chondrichthyan fish, *in* JOHANSON Z., UNDERWOOD C., RICHTER M. (eds), *Evolution and Development of Fishes*, Cambridge, UK: Cambridge University Press, pp. 110-125.

DINGERKUS G., SÉRET B., GUILBERT E., 1991. Multiple prismatic calcium phosphate layers in the jaws of present-day sharks (Chondrichthyes; Selachii). *Experientia* 47: 38-40. https://doi.org/10.1007/BF02041246

FREY L., COATES M.I., TIETJEN K., RÜCKLIN M., KLUG C., 2020. A symmoriiform from the Late Devonian of Morocco demonstrates a derived jaw function in ancient chondrichthyans. *Communications Biology* 3: 681. https://doi.org/10.1038/s42003-020-01394-2

GROGAN E., LUND R., GREENFEST-ALLEN E., 2012. The origin and relationships of early chondrichthyans, *in* CARRIER J., MUSICK J., HEITHAUS M. (eds), *Biology of Sharks and their Relatives*, Boca Raton, USA: CRC Press, pp. 3–31.

HARA E.S., OKADA M., NAGAOKA N., HATTORI T., KUBOKI T., NAKANO T., MATSUMOTO T., 2018. Bioinspired mineralisation using chondrocyte membrane nanofragments. *ACS Biomaterials Science & Engineering* 4: 617–625. https://doi.org/10.1021/acsbiomaterials.7b00962

HUBER D.R., DEAN M.N., SUMMERS A.P., 2008. Hard prey, soft jaws and the ontogeny of feeding mechanics in the spotted ratfish *Hydrolagus colliei*. *Journal of the Royal Society Interface* 5: 1867-1878. https://doi.org/10.1098/rsif.2008.0301

JOHANSON Z., UNDERWOOD C., COATES M.I., FERNANDEZ V., CLARK B., SMITH M.M., 2021. The stem-holocephalan *Helodus* (Chondrichthyes; Holocephali) and the evolution of modern chimaeroid dentitions, *in* PRADEL A., DENTON J.S.S., JANVIER P. (eds), *Ancient Fishes and Their Living Relatives: A tribute to John G Maisey*, Munich, Germany: Verlag Dr. Friedrich Pfeil, pp. 205-214.

KEMP N.E., WESTRIN S.K., 1979. Ultrastructure of calcified cartilage in the endoskeleton tesserae of sharks. *Journal of Morphology* 160: 75-102. https://doi.org/10.1002/jmor.1051600106

LANE J.A., MAISEY J.G., 2012. The visceral skeleton and jaw suspension in the durophagous hybodontid shark *Tribodus limae* from the Lower Cretaceous of Brazil. *Journal of Paleontology* 86: 886–905. https://doi.org/10.2307/23254510

LEMIERRE A., GERMAIN D., 2019. A new mineralised tissue in the early vertebrate *Astraspis*. *Journal of Anatomy* 235: 1105-1113. https://doi.org/10.1111/joa.13070

LOU F., CURTIN N.A., WOLEDGE R.C., 2002. Isometric and isovelocity contractile performance of red muscle fibres from the dogfish *Scyliorhinus canicular*. *Journal of Experimental Biology* 205: 1585–1595. https://doi.org/0.1242/jeb.205.11.1585

MAISEY J.G., MILLER R., PRADEL A., DENTON J.S.S., BRONSON A., JANVIER P., 2017. Pectoral morphology in *Doliodus*: bridging the « acanthodian » – chondrichthyan divide. *American Museum Novitates* 3875: 1-15. https://doi.org/0.1206/3875.1

MAISEY J.G., DENTON J.S.S., BURROW C., PRADEL A., 2021. Architectural and ultrastructural features of tessellated calcified cartilage in modern and extinct chondrichthyan fishes. *Journal of Fish Biology* 98: 919–941. https://doi.org/10.1111/jfb.14376

MARCONI A., HANCOCK-RONEMUS A., GILLIS J.A., 2020. Adult chondrogenesis and spontaneous cartilage repair in the skate, *Leucoroja erinacea. eLife*: 2020;9: e53414. https://doi.org/10.7554/eLife.53414 3

PAZZAGLIA U.E., REGUZZONI M., MANCONI R., ZECCA P.A., ZARATTINI G., CAMPAGNOLO M., RASPANTI M., 2022. The combined cartilage growth – calcification patterns in the wing-fins of Rajidae (Chondrichthyes): A divergent model from endochondral ossification of tetrapods. *Microscopy Research & Technique* 85: 3642–3652. https://doi.org/10.1002/jemt.24217

PAZZAGLIA U.E., REGUZZONI M., MANCONI R., ZECCA P.A., ZARATTINI G., CAMPAGNOLO M., RASPANTI M., 2022. Morphology of joints and patterns of cartilage calcification in the endoskeleton of the batoid *Raja cf. polystigma*. *Journal of Anatomy* 240: 1127-1140. https://doi.org/10.1111/joa.13623

POWELL P.L., ROY R.R., KANIM P., BELLO M.A., EDGERTON V.R., 1984. Predictability of skeletal muscle tension from architectural determinations of guinea pigs. *Journal of Applied Physiology* 57: 1715-1721. https://doi.org/10.1152/jappl.1984.57.6.1715

PRADEL A., MAISEY J.G., TAFFOREAU P., MAPES R.H., MALLATT J., 2014. A Palaeozoic shark with osteichthyan-like branchial arches. *Nature* 509: 608–611.

RINEAU V., GRAND A., ZARAGüETA R. & LAURIN M. 2015. — Experimental systematics: sensitivity of cladistic methods to polarization and character ordering schemes. *Contributions to Zoology* 84 (2): 129-148.

SEIDEL R., BLUMER M., ZASLANSKY P., KNÖTEL D., HUBER D.R., WEAVER J.C., FRATZL P., OMELON S., BERTINETTI L., DEAN M.N., 2017. Ultrastructural, material and crystallographic description of endophytic masses – A possible damage response in shark and ray tessellated calcified cartilage. *Journal of Structural Biology* 198: 5–18. https://doi.org/10.1016/j.jsb.2017.03.004

SEIDEL R., BLUMER M., CHAUMEL J., AMINI S., DEAN M.N., 2020. Endoskeletal mineralisation in chimaera and a comparative guide to tessellated cartilage in chondrichthyan fishes (sharks, rays and chimaera). *Journal of the Royal Society Interface* 17: 20200474. https://doi.org/10.1098/rsif.2020.0474

SEIDEL R., JAYASANKAR A.K., DEAN M.N., 2021. The multiscale architecture of tessellated cartilage and its relation to function. *Journal of Fish Biology* 98: 942–955. https://doi.org/ 10.1111/jfb.14444

SMITH M., MANZANARES E., UNDERWOOD C., HEALY C., CLARK B., JOHANSON Z., 2020. Holocephalan (Chondrichthyes) dental plates with hypermineralised dentine as a substitute for missing teeth through developmental plasticity. *Journal of Fish Biology* 97: 16–27. https://doi.org/10.1111/jfb.14302

SUMMERS A.P., KOOB T.J., BRAINERD E.L., 1998. Stingray jaws strut their stuff. *Nature* 395: 450-451.

SUMMERS A.P., 2000. Stiffening the stingray skeleton – An investigation of durophagy in myliobatid stingrays (Chondrichthyes, Batoidea, Myliobatidae). *Journal of Morphology* 243: 113-126. https://doi.org/10.1002/(SICI)1097-4687(200002)243:2<113::AID-JMOR1>3.0.CO;2-A

SWARTZ S.M., PARKER A., HUO C., 1998. Theoretical and empirical scaling patterns and topological homology in bone trabeculae. *Journal of Experimental Biology* 201: 573–590. https://doi.org/10.1242/jeb.201.4.573

TAKAGI M., PARMLEY R.T., DENYS F.R., YAGASAKI H., TODA Y., 1984. Ultrastructural cytochemistry of proteoglycans associated with calcification of shark cartilage. *Anatomical Record* 208: 149–158. https://doi.org/10.1002/ar.1092080202

TEITELBAUM S.L., 2000. Bone resorption by osteoclasts. *Science* 289: 1504–1508. https://doi.org/0.1126/science.289.5484.1504

WAINWRIGHT P.C., 1988. Morphology and ecology: functional basis of feeding constraints in Caribbean labrid fishes. *Ecology* 69: 635-645. https://doi.org/10.2307/1941012

WILLIANTARRA I., LEUNG S., CHOI Y.S., CHHANA A., MCGLASHAN S.R., 2022. Chondrocyte-specific response to stiffness-mediated primary cilia formation and centriole positioning. *American Journal of Physiology - Cell Physiology* 323: C236–C247. https://doi.org/10.1152/ajpcell.00135.2022

WROE S., HUBER D.R., LOWRY M., MCHENRY C., MORENO K., CLAUSEN P., FERRARA T.L., CUNNINGHAM E., DEAN M.N., SUMMERS A.P., 2008. Three-dimensional computer analysis of white shark jaw mechanics: how hard can a great white bite? *Journal of Zoology* 276: 336–342. https://doi.org/10.1111/j.1469-7998.2008.00494.x

ZOETIS T., TASSINARI M.S., BAGI C., WALTHALL K., HURTT M.E., 2003. Species comparison of postnatal bone growth and development. *Birth Defects Research Part B* 68: 86–110. https://doi.org/10.1002/bdrb.10012

Supplementary material

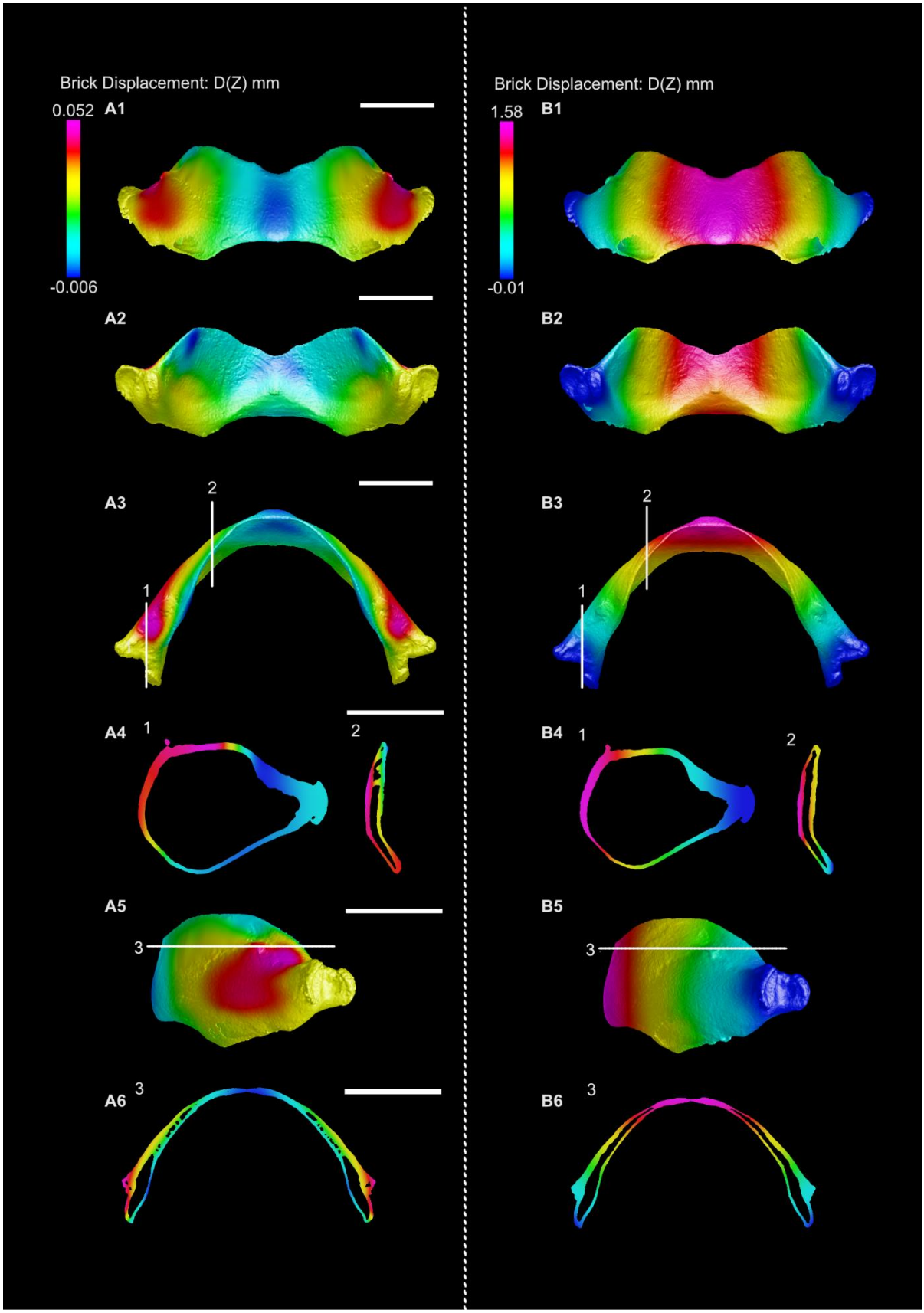

Supplementary Figure 1: Brick displacement along the vertical (Z) axis in the lower jaw (Meckel's cartilage) due to biting in the adult specimen of *Chimaera monstrosa* (MNHN-2022-362). A1-B1: Anterior view, A2-B2: Posterior view, A3-B3: Dorsal view, A4-B4: Transversal cross-sectional views, A5-B5: Left lateral view, A6-B6: Longitudinal cross section. Scale bars: 1cm.

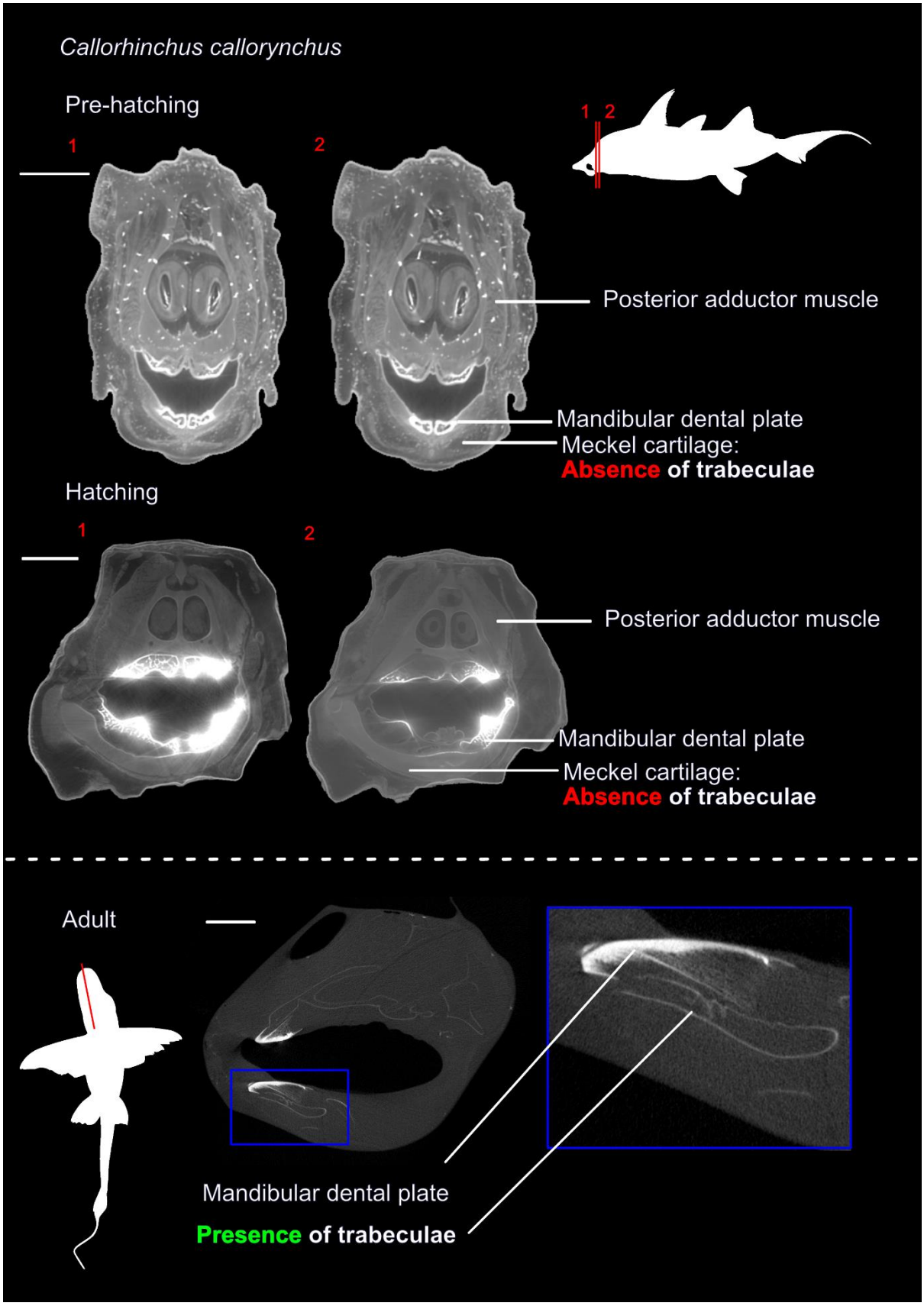

Supplementary Figure 2: Ontogenetic growth of the Meckel cartilage in *Callorhinchus callorhynchus*. The embryos (both pre-hatching and hatchling) were captured in the San Matías Gulf (Patagonia, Argentina, 2013). The specimens were fixed in a 10% formaldehyde solution and then preserved in a 96% ethanol solution for scanning at the European Synchrotron Radiation Facilities (ESRF) in Grenoble (France). This sampling was organized within a collaborative program between the Instituto de Biología Marina y Pesquera Alte Storni (San Antonio Oeste, Rio Negro, Argentina), the American Museum of Natural History (New-York City, USA), the Laboratoire Evolution Génomes Comportement Ecologie (Paris, France), the Muséum National d'Histoire Naturelle (Paris, France) and the Medical University of South Carolina, Marine Genomics (USA). The adult specimen (SIO 64-483) was provided by Adam Summers and was scanned by Matt Kolmann at the Scripps Museum (California, USA).

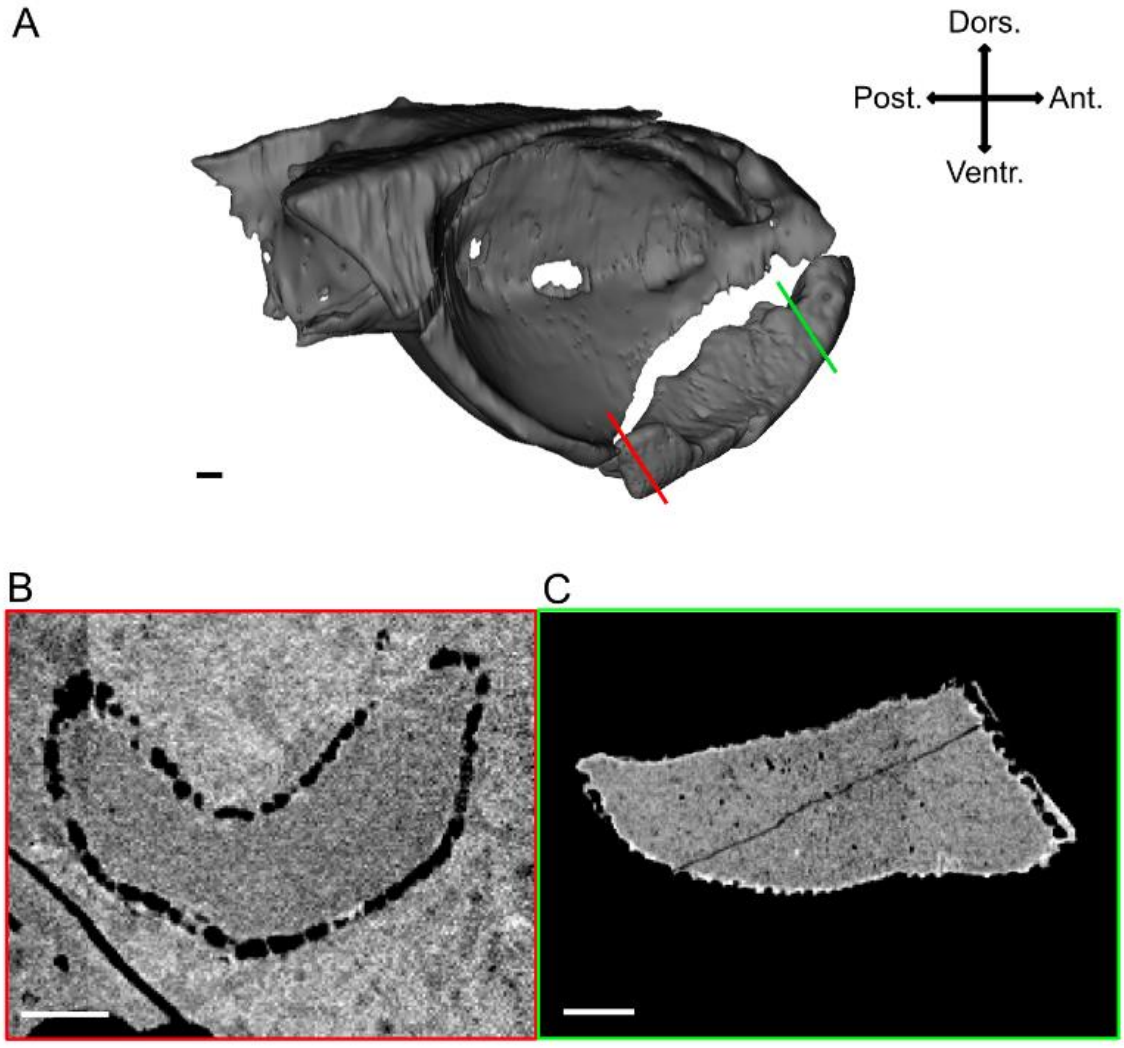

Supplementary Figure 3: A. Right lateral view of the skull of *Iniopera* sp. (KUVP 22060), the Upper Pennsylvanian (late Virgilian, 305 to 299 Ma) Haskell Formation, Kansas, US. B. Transversal cross section of the posterior part of the lower jaw. C. Transversal cross section of the anterior part of the lower jaw. Abbreviations: Ant. : Anterior, Post. : Posterior, Dors. : Dorsal, Ventr. : Ventral. Scale bars: 1mm.

Chimaera monstrosa (MNHN-2022-362)					
Cranial muscles	Weight (gr.)	Pennation angle (rad)	Mean Fibre Length (cm)	Muscle density (g/cm^3)	PCSA (cm^2)
M. Epiaxialis	1.58	0	1.95	1.05	0.77
M. Protractor dorsalis pectoralis	1.69	0.35	1.34	1.05	1.13
M. Retractor latero-ventralis pectoralis	1.97	0.785	1.86	1.05	0.72
M. Constrictor operculi dorsalis anterior	0.74	0.35	1.89	1.05	0.35
M. Constrictor operculi dorsalis	1.75	2.18	2.47	1.05	0.39
M. Cucullaris superficialis	2.66	0	1.73	1.05	1.47
M. Adductor mandibulae anterior	5.26	0.52	2.05	1.05	2.11
M. Levator anguli oris anterior	0.51	0	2.90	1.05	0.17
M. Levator anguli oris posterior	3.47	0	2.54	1.05	1.30
M. Adductor mandibulae posterior	0.70	0.52	1.10	1.05	0.53
M. Constrictor operculi ventralis	2.10	0.70	2.83	1.05	0.54
M. Coracomandibularis	3.46	0.087	3.00	1.05	1.10
M. Coracohyoideus	1.00	0	2.00	1.05	0.48
mm. Coracobranchiales	6.91	0.87	1.78	1.05	2.38

Supplementary Table 1: Cranial muscle characteristics of the adult specimen of *Chimaera monstrosa* (MNHN-2022-362; after dissection, see material and methods for details). Abbreviation: P_{CSA}: Physiological Cross Section Area.

Jaw adductor muscles	PCSA (cm^2)	TSPR (kNm^{-2}	Po (N)	$\cos\alpha$			Force components (N)		
				X	Y	Z	X	Y	Z
L Anterior	2.11	142	30	-0.67	-0.19	0.717	-20.15	-5.61	21.51
L Posterior	0.525	142	7.46	-0.97	0.22	0.11	-7.23	1.601	0.82
R Anterior	2.11	142	30	-0.67	0.19	0.72	-20.15	5.61	21.51
R Posterior	0.525	142	7.46	-0.97	-0.22	0.11	-7.23	-1.61	0.82

Supplementary Table 2: Calculation of the jaw adductor muscle force components in the adult specimen of *Chimaera monstrosa* (MNHN-2022-362). Symbols and abbreviations: P_{CSA}: Physiological Cross Section Area, T_{SPR}: the specific tension of elasmobranch red muscle, P_o: the muscle theoretical maximum tetanic force. α: the angle between the muscle vector and each axis at the muscle insertion on the lower jaw.